TYPE-1 AND TYPE-2 FUZZY CONTROL OF AN ANTI-LOCK BREAKING SYSTEM (ABS) AND EVALUATION OF ITS PERFORMANCES

Ayse Cisel Aras[1], Yesim Oniz[1], Okyay Kaynak[1] and Rahib Abiyev[2]
[1]*Department of Electrical and Electronics Engineering, Bogazici University, Istanbul, Turkey*
[2]*Department of Computer Engineering, Near East University, Lefkosa, North Cyprus*

Keywords: Antilock braking system, Type-1 fuzzy neuro system, Type-2 fuzzy neuro system, Gradient descent algorithm.

Abstract: The control of nonlinear systems is a challenging task in control engineering and the use of type-1 Fuzzy Logic Controllers (FLCs) has been proposed as a possible approach. However, traditional type-1 FLCs can prove to be inadequate in dynamically unstructured environments that include large amount of uncertainties. Under such circumstances, type-2 fuzzy logic controllers can be a viable alternative. In this paper, an Anti-Lock Breaking System (ABS) is controlled both by a type-1 and an interval type-2 fuzzy logic controller with and without noisy input measurement. The performances of both controllers are approximately the same without noise in the input measurement. However, with noisy input measurements, interval type-2 fuzzy logic controller results in better performance, indicating its superiority when there exist considerable amount of uncertainties in the system to be controlled.

1 INTRODUCTION

Type-1 Fuzzy Logic Systems (T1-FLSs) were first introduced by Zadeh in 1965, and since then the area has drawn the interest of many scientists and been extensively used for modeling and control purposes. In literature, there are noteworthy studies that have used type-1 Fuzzy Logic Controllers (FLCs) as referenced in a recent survey paper (Precup and Hellendoorn, 2011).

In most real world applications, the control engineers are confronted with uncertainties and imprecise information due to the internal and the external dynamics of the system to be controlled. Type-1 fuzzy logic controllers may prove to be inefficient in handling these kinds of uncertainties. To overcome the problem, the use of type-2 FLCs is suggested in the literature and many successful applications are reported (Hagras, 2007), (Liang and Mendel, 2000). Most of these are based on interval type-2 (IT2) structures (Abiyev and Kaynak, 2010),(Castillo and Melin, 2008).

In this study, uncertainty and noise handling capability of the considered IT2 FLCs is investigated. The rule-base of IT2 Fuzzy Neuro System (FNS) structure is of TSK type. The antecedent part of the fuzzy IF-THEN rules is composed of interval type-2 membership functions and the consequent part is a first order polynomial. The design parameters in the antecedent part are the centers and the standard deviations of the Gaussian membership functions. Their means are assumed to be uncertain. The design parameters in the consequent part are the coefficients of the first order polynomial. These parameters of the structure are tuned by using gradient descent algorithm.

In Section 2, the mathematical description of the ABS system used as the test bed is presented. In Section 3, the structure of the type-2 fuzzy neural system is described and parameter update rules are derived. The simulation studies carried out on the ABS system are presented in Section 4. In Section 5, an analysis of the results is given and the further work in the area is discussed.

2 THE MATHEMATICAL DESCRIPTION OF ABS SYSTEM

To derive the mathematical model of the ABS, the free body diagram of the quarter vehicle model shown in

Cisel Aras A., Oniz Y., Kaynak O. and Abiyev R..
TYPE-1 AND TYPE-2 FUZZY CONTROL OF AN ANTI-LOCK BREAKING SYSTEM (ABS) AND EVALUATION OF ITS PERFORMANCES.
DOI: 10.5220/0003645505030508
In *Proceedings of the 8th International Conference on Informatics in Control, Automation and Robotics* (ICM-2011), pages 503-508
ISBN: 978-989-8425-74-4

Table 1: System Parameters.

ω_1	Angular velocity of the upper wheel
ω_2	Angular velocity of the lower wheel
T_B	Braking torque
r_1	Radius of the upper wheel
r_2	Radius of the lower wheel
J_1	Moment of inertia of the upper wheel
J_2	Moment of inertia of the lower wheel
d_1	Viscous friction coefficient of the upper wheel
d_2	Viscous friction coefficient of the lower wheel
F_n	Total normal load
μ	Road adhesion coefficient
λ	Wheel slip
F_t	Road friction force
M_{10}	Static friction of the upper wheel
M_{20}	Static friction of the lower wheel

Fig. 1 is considered. The model is quite simple, but it maintains the fundamental characteristics of a real system. The lower wheel imitates the relative road motion, whereas the upper wheel, mounted to the balance lever, animates the wheel of the vehicle. Several assumptions are made in deriving the dynamic equations of the system: The lateral and vertical motions of the vehicle have been neglected and only the longitudinal dynamics have been considered. Additionally, it is assumed that there is no interaction between the four wheels of the vehicle.

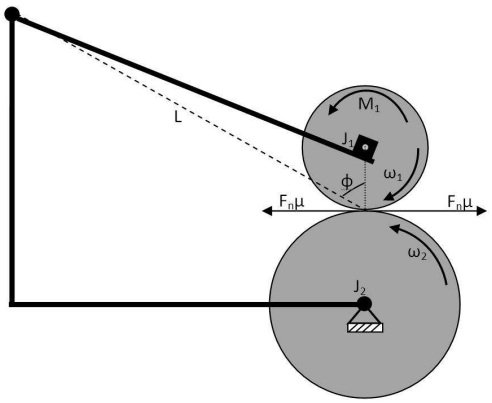

Figure 1: Schematic view of experimental setup.

Regarding Fig.1, three torques act on the upper wheel. These are the braking torque, the friction torque in the upper bearing, and the friction torque among the wheels. Similarly, two torques act on the lower wheel, which are the friction torque in the lower bearing and the friction torque between these wheels. For braking, a torque is applied to the upper wheel, which causes the wheel to slow down. According to the Newton's second law, the equation of the motion of the system can be written as:

$$J_1\dot{\omega}_1 = F_t r_1 - (d_1\omega_1 + M_{10} + T_B) \quad (1)$$

$$J_2\dot{\omega}_2 = -(F_t r_2 + d_2\omega_2 + M_{20}) \quad (2)$$

In these equations F_t can be stated as

$$F_t = \mu(\lambda)F_n \quad (3)$$

The normal force, F_n, is computed with the following formula:

$$F_n = \frac{d_1\omega_1 + M_{10} + T_B + M_g}{L(\sin\phi - \mu(\lambda)\cos\phi)} \quad (4)$$

In Eq. (4), L is the distance between the contact point of the wheels and the rotational axis of the balance lever and Φ corresponds to the angle between the normal in the contact point and the line L. During driving, the speed of the vehicle and the rotational velocity of the wheel have matching values. However, during braking, the braking torque is generated at the interface between the wheel and road surface, which causes the wheel speed to decrease. Consequently, the wheel speed will tend to be lower than vehicle speed. The parameter used to specify this difference in these velocities is called wheel slip and denoted by λ.

$$\lambda = \frac{r_2\omega_2 - r_1\omega_1}{r_2\omega_2} \quad (5)$$

A zero wheel slip means that the wheel velocity is equal to the speed of the car, whereas a ratio of one indicates that the wheel is not rotating, but the car is still moving, i.e. the wheels are skidding on the road and the vehicle is no more steerable. The road adhesion coefficient is a nonlinear function of some physical variables including wheel slip and it can be approximated by the following formula (Inteco, 2007):

$$\mu(\lambda) = \frac{c_4\lambda^p}{a+\lambda^p} + c_3\lambda^3 + c_2\lambda^2 + c_1\lambda \quad (6)$$

The resulting road adhesion coefficient vs. wheel slip curve is presented in Fig. 2. As can be seen from this figure, a wheel slip value of 0.2 corresponds to the maximum value of the road adhesion coefficient.

The numerical values used in this study for the simulations are:

$r_1 = 0.0995(m)$
$r_2 = 0.0990(m)$
$\phi = 65.61(^\circ)$
$L = 0.37(m)$
$J_1 = 0.00753(kgm^2)$
$J_2 = 0.0256(kgm^2)$
$d_1 = 0.00011874(kgm^2/s)$
$d_2 = 0.00021468(kgm^2/s)$
$M_{10} = 0.0032(Nm)$
$M_{20} = 0.0925(Nm)$
$c_1 = -0.04240011450454$,
$c_2 = 0.00000000029375$,
$c_3 = 0.03508217905067$,
$c_4 = 0.40662691102315$,
$a = 0.00025724985785$, and
$p = 2.09945271667129$.

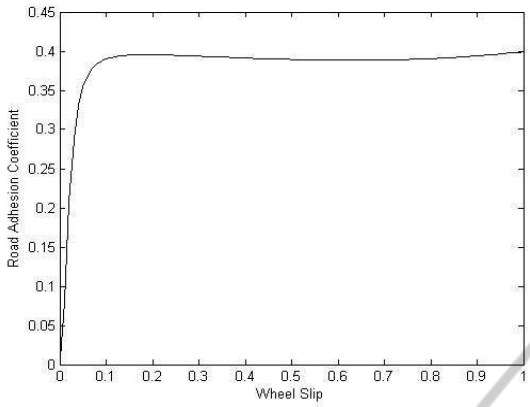

Figure 2: Road adhesion coefficient vs. wheel slip.

3 THE THEORETICAL AND MATHEMATICAL BACKGROUND OF T2-FNS

In real world applications, systems experience many uncertainties due to the dynamically unstructured environments. Traditional fuzzy logic systems may not be able to handle these kind of uncertainties. In this study a type-2 fuzzy-neuro structure is used as the controller of a system which has two inputs, the error (e) and the derivative of the error ($\triangle e$). The structure of the MISO (multi-input, single-output) neuro fuzzy controller is given in Fig. 3.

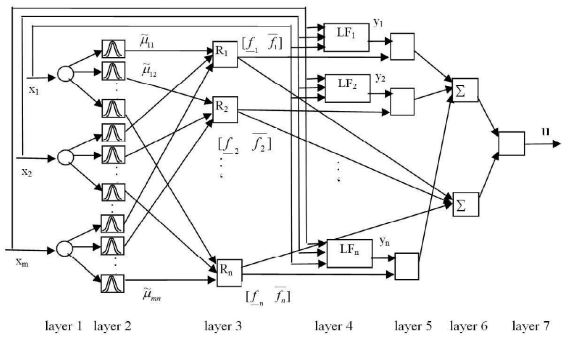

Figure 3: The structure of neuro-fuzzy inference system.

This structure is constructed as a IT2 TSK fuzzy logic system. Such systems are divided in the literature into three models depending on the types of membership functions on the antecedent and the consequent parts of the fuzzy IF-THEN rules (Liang and Mendel, 1999). This work focusses on the second model.

In Fig. 3, the first layer of the network is fed by the external input signal, $X = x_1, x_2, ..., x_n$. In the second layer, the input space is defined by using Gaussian membership functions with uncertain mean which are initially distributed onto the input domain equally as shown in Fig. 4.

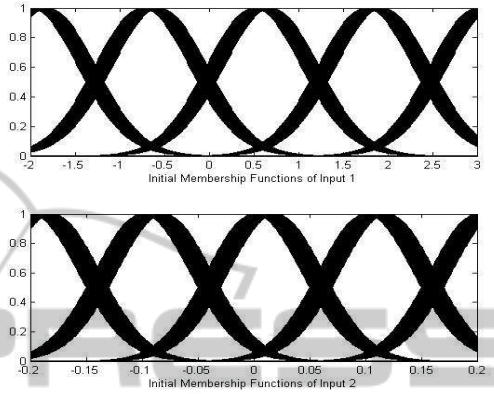

Figure 4: Initial interval type-2 Gaussian membership functions with uncertain mean.

The fuzzy IF-THEN rule structure has the following form:

$$\text{IF } x_1 \text{ is } \tilde{\tilde{A}}_{1j} \text{ and...and } x_m \text{ is } \tilde{\tilde{A}}_{mj} \text{ THEN } y_j \text{ is } \sum_{i=1}^{m} w_{ij}x_i + b_j \tag{7}$$

where $x_i (i = 1, ..., m)$ are the input variables, $y_j (j = 1, ..., n)$ are the output variables which are the linear functions. The antecedent part of the rule is composed of interval type-2 fuzzy sets, $\tilde{\tilde{A}}_{ij}$ for the j-th rule of the i-th input, and the consequent part of the rule is a first order polynomial with the coefficients, w_{ij} and b_j.

The second layer in Fig. 3, the upper and lower membership functions degrees are determined by using Eq. (8).

$$\mu_{\tilde{A}_k^i} = [\underline{\mu}_{\tilde{A}_k^i}(x_k), \overline{\mu}_{\tilde{A}_k^i}(x_k)] = [\underline{\mu}^i, \overline{\mu}^i] \tag{8}$$

Lower and upper membership functions between i^{th} input and j^{th} hidden neurons of layer 3 can be given as follows:

$$\underline{\mu}_{ij}(x) = \begin{cases} G(c2_{ij}, \sigma_{ij}, x_i) & x_i \leq \frac{c1_{ij}+c2_{ij}}{2} \\ G(c1_{ij}, \sigma_{ij}, x_i) & x_i > \frac{c1_{ij}+c2_{ij}}{2} \end{cases}$$

$$\underline{\mu}_{ij}(x) = \begin{cases} G(c1_{ij}, \sigma_{ij}, x_i) & x_i < c1_{ij} \\ 1 & c1_{ij} \leq x_i \leq c2_{ij} \\ G(c2_{ij}, \sigma_{ij}, x_i) & x_i > c2_{ij} \end{cases} \tag{9}$$

where $G(c_{ij},\sigma_{ij},x_i)$ is determined as:

$$G(c_{ij},\sigma_{ij},x_i) = exp\left(-\frac{1}{2}\frac{(x_i-c_{ij})^2}{\sigma_{ij}^2}\right) \quad (10)$$

The firing strengths of the rules are calculated by using the prod t-norm operator at the third layer.

$$\underline{f} = \underline{\mu}_{\tilde{A}_1}(x_1) * \cdots * \underline{\mu}_{\tilde{A}_n}(x_n) \quad (11)$$

$$\overline{f} = \overline{\mu}_{\tilde{A}_1}(x_1) * \cdots * \overline{\mu}_{\tilde{A}_n}(x_n) \quad (12)$$

The output of the consequent part of the each rule is calculated at the fourth layer as follows:

$$y_j = \sum_{i=1}^{m} w_{ij}x_i + b_j \quad (13)$$

The type reduction and the defuzzification procedures are realized at the fifth, the sixth and the seventh layers of the neuro-fuzzy structure. The defuzzified output of the type-2 TSK fuzzy system is determined by using the inference engine proposed in (Biglarbegian et al., 2010), and has the following form:

$$u = \frac{p\sum_{j=1}^{N}\underline{f}_j y_j}{\sum_{j=1}^{N}\underline{f}_j} + \frac{q\sum_{j=1}^{N}\overline{f}_j y_j}{\sum_{j=1}^{N}\overline{f}_j} \quad (14)$$

where $\underline{f}_j$ and $\overline{f}_j$ are the lower and upper firing strength of each rule, respectively. p and q are the design parameters that weight the sharing of lower and upper firing levels of each fired rule, N is the number of rules.

4 TRAINING OF THE T2-FNS

After the output of the system is calculated, the gradient descent algorithm is applied to tune the design parameters of the system which are the center and the standard deviation of the membership functions at the antecedent part, the coefficients of the first order polynomial at the consequent part, p and q values in Eq. (14).

Initially, the output error is determined as follows:

$$E = \frac{1}{2}\sum_{i=1}^{O}(u_i^d - u_i)^2 \quad (15)$$

where O is the number of output, u_i^d and u_i are the desired and the actual output of the network, respectively.

The parameters at the antecedent part of the rules, $c1_{ij}$, $c2ij$, σ_{ij} and the parameters at the consequent part of the rules, w_{ij}, b_j are tuned by using gradient descent algorithm as follows:

$$w_{ij}(t+1) = w_{ij}(t) - \gamma\frac{\partial E}{\partial w_{ij}}; b_j(t+1) = b_j(t) - \gamma\frac{\partial E}{\partial b_j} \quad (16)$$

$$c1_{ij}(t+1) = c1_{ij}(t) - \gamma\frac{\partial E}{\partial c1_{ij}}; c2_{ij}(t+1) = c2_{ij}(t) - \gamma\frac{\partial E}{\partial c2_{ij}} \quad (17)$$

$$\sigma_{ij}(t+1) = \sigma_{ij}(t) - \gamma\frac{\partial E}{\partial \sigma_{ij}} \quad (18)$$

where γ is the learning rate. The derivatives in Eqs. 16-18 are determined as follows:

$$\frac{\partial E}{\partial w_{ij}} = \frac{\partial E}{\partial u}\frac{\partial u}{\partial y_j}\frac{\partial y_j}{\partial w_{ij}} \quad (19)$$

$$\frac{\partial E}{\partial b_j} = \frac{\partial E}{\partial u}\frac{\partial u}{\partial y_j}\frac{\partial y_j}{\partial b_j} \quad (20)$$

$$\frac{\partial E}{\partial \sigma_{ij}} = \sum_j \frac{\partial E}{\partial u}\left[\frac{\partial u}{\partial \underline{f}_j}\frac{\partial \underline{f}_j}{\partial \underline{\mu}_{ij}}\frac{\partial \underline{\mu}_{ij}}{\partial \sigma_{ij}} + \frac{\partial u}{\partial \overline{f}_j}\frac{\partial \overline{f}_j}{\partial \overline{\mu}_{ij}}\frac{\partial \overline{\mu}_{ij}}{\partial \sigma_{ij}}\right]$$

$$\frac{\partial E}{\partial c1_{ij}} = \sum_j \frac{\partial E}{\partial u}\left[\frac{\partial u}{\partial \underline{f}_j}\frac{\partial \underline{f}_j}{\partial \underline{\mu}_{ij}}\frac{\partial \underline{\mu}_{ij}}{\partial c1_{ij}} + \frac{\partial u}{\partial \overline{f}_j}\frac{\partial \overline{f}_j}{\partial \overline{\mu}_{ij}}\frac{\partial \overline{\mu}_{ij}}{\partial c1_{ij}}\right]$$

$$\frac{\partial E}{\partial c2_{ij}} = \sum_j \frac{\partial E}{\partial u}\left[\frac{\partial u}{\partial \underline{f}_j}\frac{\partial \underline{f}_j}{\partial \underline{\mu}_{ij}}\frac{\partial \underline{\mu}_{ij}}{\partial c2_{ij}} + \frac{\partial u}{\partial \overline{f}_j}\frac{\partial \overline{f}_j}{\partial \overline{\mu}_{ij}}\frac{\partial \overline{\mu}_{ij}}{\partial c2_{ij}}\right]$$

where

$$\frac{\partial E}{\partial u} = u(t) - u^d(t); \frac{\partial u}{\partial \underline{f}_j} = p\frac{y_j - \underline{u}}{\sum_{j=1}^{n}\underline{f}_j}; \frac{\partial u}{\partial \overline{f}_j} = q\frac{y_j - \overline{u}}{\sum_{j=1}^{n}\overline{f}_j}$$

$$\underline{u} = \frac{\sum_{j=1}^{n}\underline{f}_j y_j}{\sum_{j=1}^{n}\underline{f}_j}; \overline{u} = \frac{\sum_{j=1}^{n}\overline{f}_j y_j}{\sum_{j=1}^{n}\overline{f}_j} \quad (21)$$

t-norm *prod* operator has the following form.

$$\frac{\partial \underline{f}_j}{\partial \underline{\mu}_{ij}} = \prod_{\substack{k=1 \\ k\neq i}}^{N1} \underline{\mu}_{kj} \quad (22)$$

$$\frac{\partial \overline{f}_j}{\partial \overline{\mu}_{ij}} = \prod_{\substack{k=1 \\ k\neq i}}^{N1} \overline{\mu}_{kj} \quad (23)$$

where $i =, ..., N1, k = 1, ..., N1$, and $j = 1, ..., N2$.

Then,

$$\frac{\partial \overline{\mu}_j(x_i)}{\partial c1_{ij}} = \begin{cases} G(c1_{ij},\sigma_{ij},x_i)\frac{(x_i - c1_{ij})}{\sigma_{ij}^2}, & x_i < c1_{ij} \\ 0, & c1_{ij} \le x_i \le c2_{ij} \\ 0, & x_i > c2_{ij} \end{cases}$$

$$\frac{\partial \underline{\mu}_j(x_i)}{\partial c1_{ij}} = \begin{cases} 0, & x_i \le \frac{c1_{ij}+c2_{ij}}{2} \\ G(c1_{ij},\sigma_{ij},x_i)\frac{(x_i-c1_{ij})}{\sigma_{ij}^2}), & x_i > \frac{c1_{ij}+c2_{ij}}{2} \end{cases} \tag{24}$$

$$\frac{\partial \overline{\mu}_j(x_i)}{\partial c2_{ij}} = \begin{cases} 0, & x_i < c1_{ij} \\ 0, & c1_{ij} \le x_i \le c2_{ij} \\ G(c2_{ij},\sigma_{ij},x_i)\frac{(x_i-c2_{ij})}{\sigma_{ij}^2}, & x_i > c2_{ij} \end{cases}$$

$$\frac{\partial \underline{\mu}_j(x_i)}{\partial c2_{ij}} = \begin{cases} G(c2_{ij},\sigma_{ij},x_i)\frac{(x_i-c2_{ij})}{\sigma_{ij}^2}), & x_i \le \frac{c1_{ij}+c2_{ij}}{2} \\ 0, & x_i > \frac{c1_{ij}+c2_{ij}}{2} \end{cases} \tag{25}$$

$$\frac{\partial \overline{\mu}_j(x_i)}{\partial \sigma_{ij}} = \begin{cases} G(c1_{ij},\sigma_{ij},x_i)\frac{(x_i-c1_{ij})^2}{\sigma_{ij}^3}, & x_i < c1_{ij} \\ 0, & c1_{ij} \le x_i \le c2_{ij} \\ G(c2_{ij},\sigma_{ij},x_i)\frac{(x_i-c2_{ij})^2}{\sigma_{ij}^3}, & x_i > c2_{ij} \end{cases}$$

$$\frac{\partial \underline{\mu}_j(x_i)}{\partial \sigma_{ij}} = \begin{cases} G(c2_{ij},\sigma_{ij},x_i)\frac{(x_i-c2_{ij})^2}{\sigma_{ij}^3}), & x_i \le \frac{c1_{ij}+c2_{ij}}{2} \\ G(c1_{ij},\sigma_{ij},x_i)\frac{(x_i-c1_{ij})^2}{\sigma_{ij}^3}), & x_i > \frac{c1_{ij}+c2_{ij}}{2} \end{cases} \tag{26}$$

The parameters p and q enable us to adjust the lower and upper portions of the final output in Eq. (14). The optimization algorithm for these parameters is given by the following equations. The initial value for both parameters is taken as 0.5.

$$p(t+1) = p(t) - \gamma\frac{\partial E}{\partial p} \tag{27}$$

$$q(t+1) = q(t) - \gamma\frac{\partial E}{\partial q} \tag{28}$$

where

$$\frac{\partial E}{\partial p} = (u-u^d)\frac{\underline{f}_j}{\sum_{j=1}^n \underline{f}_j} \tag{29}$$

$$\frac{\partial E}{\partial q} = (u-u^d)\frac{\overline{f}_j}{\sum_{j=1}^n \overline{f}_j} \tag{30}$$

5 SIMULATION RESULTS

A number of simulation studies are carried out with type-1 and type-2 FNS controllers acting on the ABS system described and the results obtained are compared. The block diagram of the type-2 FNS system is shown in Fig. 5. As has been discussed earlier, the FNS block has two inputs, e is the error and $\triangle e$ is the derivative of the error. g is the reference signal, u is the control input signal and y is the output of the system.

In the simulations, the sampling time is set to $1ms$. The rotational velocity of the upper and lower wheels before the braking operation is selected 250 *rad/s*. The reference wheel slip is set to 0.2 which corresponds to the peak value of $\mu - \lambda$. In order to determine the efficiency and the accuracy of the proposed controller two sets of simulation studies have been conducted. In the first study, the performances of both controllers are tested without noise in the input measurement. Then, in the second set of simulations, the noise effect is included as shown in Fig. 6. The signal-to-noise ratio (SNR) is about 17dB.

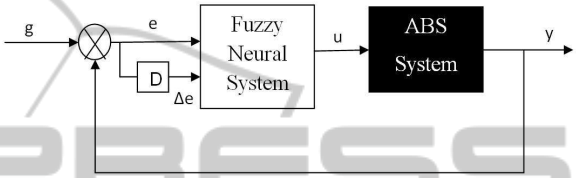

Figure 5: The structure of type-2 Neuro Fuzzy System.

The initial membership functions for error and the derivative of the error are distributed equally onto the input domain. The initial weights of the neural network are selected randomly.

Table 2 shows Root Mean Squared Error (RMSE) values to compare the performances of the both algorithms.

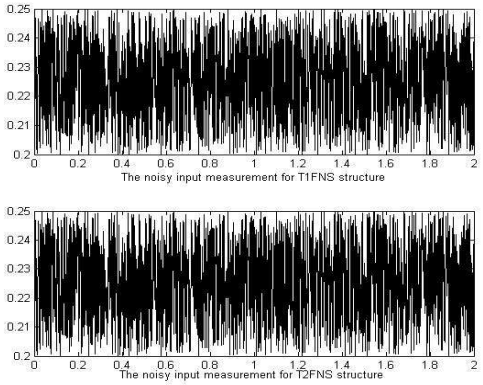

Figure 6: The noisy input measurement for the two cases.

Table 2: Root Mean Squared Error values of the type-1 and type-2 FNS algorithms.

	without Noise	**with Noise**
T1 FNS	1.731	2.419
IT2 FNS	1.714	2.197

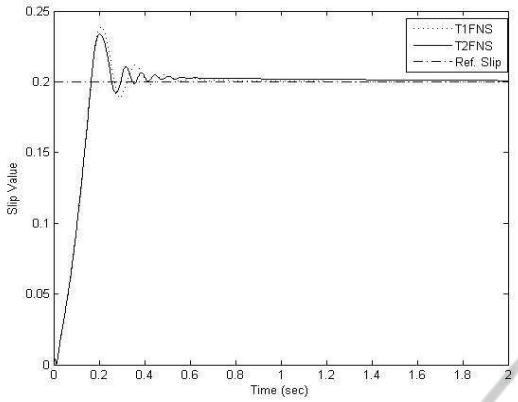

Figure 7: Wheel slip of type-1 and type-2 FNS without noise in the input measurement.

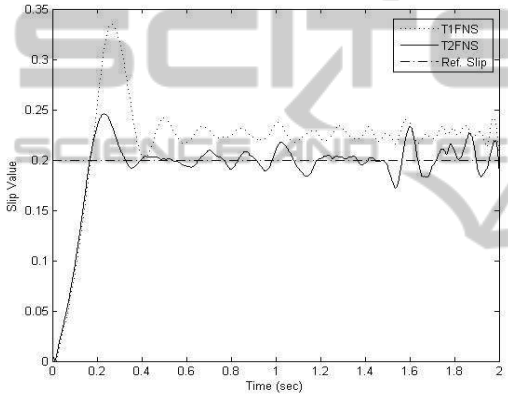

Figure 8: Wheel slip of type-1 and type-2 FNS with noise in the input measurement.

6 CONCLUSIONS

In this paper, two different structures, a type-1 and a type-2 structure are used to control ABS system. The functions of the layers in each structure are explained in detail and the parameter update rules of the structures are given which are based on gradient descent algorithms.

A number of simulation studies are carried out. Firstly, it is assumed that the input measurements are not corrupted with noise. The results indicate that both controllers have similar responses. However, in real life, the measurements usually include some level of noise. To simulate this, a band limited white noise is added to the slip measurement. In this case, it can be seen from Fig. 8 that type-2 FNS outperforms type-1 FNS. It can therefore be concluded that type-2 FNS structure results in a better performance when there exists uncertainties. Encouraged by the simulation results, an experimental study is about to be launched.

ACKNOWLEDGEMENTS

The authors would like to acknowledge TUBITAK Grant No: 107E284 and Bogazici University Project Grant No: 08A204.

REFERENCES

Abiyev, R. and Kaynak, O. (2010). Type-2 fuzzy neural system structure for identification and control of time-varying plants. In *IEEE Trans. Indust. Electron.* vol.57, no.12, pp.4147-4159.

Biglarbegian, M., Melek, W., and Mendel, J. (2010). On the stability of interval type-2 TSK fuzzy logic control systems. In *IEEE Transactions on Systems, Man, and Cybernetics, Part B: Cybernetics*. vol.40, issue 3, pp. 798-818.

Castillo, O. and Melin, P. (2008). *Type-2 Fuzzy Logic: Theory and Applications, Studies in Fuzziness and Soft Computing*. Springer, Vol. 223.

Hagras, H. (2007). Type-2 FLCs: A new generation of fuzzy controllers. In *IEEE Computational Intelligence Magazine*. vol.2, pp.30-43.

Inteco (2007). *The Laboratory Antilock Braking System Controlled from PC*. Inteco Ltd., Poland, user's manual edition.

Liang, Q. and Mendel, J. (1999). An introduction to type-2 TSK fuzzy logic systems. In *IEEE International Fuzzy Systems Conference*. vol.3, pp. 1534-1539.

Liang, Q. and Mendel, J. (2000). Interval type-2 fuzzy logic systems: Theory and design. In *IEEE Transactions on Fuzzy Systems*. vol.8, pp.535-550.

Precup, R. and Hellendoorn, H. (2011). A survey on industrial applications of fuzzy control. In *Computers in Industry*. vol.62, pp.213-226.